electronics

MDPI

Article

Fully Polarized Wideband Omnidirectional RF Harvester with Highly Efficient DC Power Combination

Jianwei Jing [1,2], Bo Yang [2,*], Liping Yan [1], Naoki Shinohara [2] and Changjun Liu [1,*]

[1] The School of Electronics and Information Engineering, Sichuan University, Chengdu 610065, China; jingjianwei@ieee.org (J.J.); liping_yan@scu.edu.cn (L.Y.)
[2] The Research Institute for Sustainable Humanosphere, Kyoto University, Uji 611-0011, Japan; shino@rish.kyoto-u.ac.jp
* Correspondence: yang.bo.82x@kyoto-u.jp (B.Y.); cjliu@ieee.org (C.L.)

Abstract: In this work, an omnidirectional RF energy harvester with wideband coverage (1.5–2.7 GHz), all-polarization, and high-efficiency DC combining is proposed. The harvester integrates six microstrip rectenna elements with varying directions and polarizations. The harvester strategically combines six microstrip rectenna elements with different orientations and polarizations to enhance the stability of omnidirectional energy harvesting. The rectifier employs impedance compression matching techniques, incorporating open-circuited and short-circuited transmission lines to achieve a compact, broadband rectification. Experimental results show that the rectifier maintains an RF-to-DC conversion efficiency exceeding 50% within a bandwidth of 1.5 GHz to 2.7 GHz at an input power of 0 dBm, achieving a maximum efficiency of 62%. The maximum DC-combining efficiency of the rectifier array reaches 92%. These findings indicate that the harvester performs effectively with RF energy of all polarizations from various directions.

Keywords: antenna; rectifier; DC combining; wideband; omnidirectional; RF harvester

Citation: Jing, J.; Yang, B.; Yan, L.; Shinohara, N.; Liu, C. Fully Polarized Wideband Omnidirectional RF Harvester with Highly Efficient DC Power Combination. *Electronics* **2024**, *13*, 4891. https://doi.org/10.3390/electronics13244891

Academic Editor: Dimitra I. Kaklamani

Received: 1 November 2024
Revised: 27 November 2024
Accepted: 9 December 2024
Published: 11 December 2024

1. Introduction

With the rapid development of wireless communication techniques, the demand for battery-less wireless power charging circuits for wireless power transmission (WPT) and wireless energy harvesting (WEH) has increased significantly [1]. Several ambient WEH techniques have been developed for electronic device charging, including solar, temperature, and RF energies [2]. Among these solutions, RF energy harvesting offers unique merits because they are ubiquitously available from digital TV broadcasts and Wi-Fi in domestic environments, regardless of the time [3]. RF energy harvesting uses rectenna technology, where a rectenna is composed of an antenna to collect RF power and a rectifier to convert RF power into DC power [4].

Ambient RF signals are characterized by multiple frequencies, random distributions, diverse paths, and varying polarizations. Relying on uniform rectennas or arrays to capture ambient RF energy faces significant challenges due to the complexity and variability of RF environments. In [5], a curved structure was used to achieve multi-band and omnidirectional energy harvesting. However, the energy collection capability in the horizontal direction at the end of the antenna could be weakened. To achieve more omnidirectional and multi-polarized performance, an array configuration is needed.

More recently, rectennas with multi-beam, multi-polarization, or multi-bands have achieved omnidirectional harvesting capabilities, aiming to capture increased RF energy from the ambient environment [6–14]. In [6], an omnidirectional rectenna array was reported, which combined 12 single Vivaldi slot rectennas arranged in a circular pattern on the same plane, with a capturable angle range of 360°. A multi-port pixel rectenna with a triple-port rectifier was also proposed to enable omnidirectional harvesting [7]. Although the array has two polarization directions, the energy collection performance in the vertical

direction is not ideal. Optimizing the arrangement of array elements and incorporating more flexible polarization methods could improve energy collection in different directions. Additionally, expanding the bandwidth or introducing more polarization modes may help enhance the efficiency of omnidirectional energy harvesting.

The configuration of the array plays a crucial role in determining the efficiency of RF-to-DC conversion in rectenna arrays, which can be classified into three types: RF combing [8], DC combining [9], and hybrid manner [10]. The RF combining offers higher gain than DC combining, allowing antennas to effectively focus RF energy in the main beam direction, making it particularly suitable for long-distance WPT [11]. However, the high gain of RF antennas makes them highly sensitive to the direction of incident RF. Complex feeding networks needed for RF combining can increase manufacturing costs and volume. In contrast, DC combining synthesizes each rectenna unit output into DC, achieving miniaturization, simple structure, array flexibility, and direction insensitivity [6,12].

In omnidirectional harvesting of microwave power in the environment, each element exhibits varying characteristics in terms of power density, incident angle, and polarization direction [13–15]. This variability can lead to energy loss due to the unstable DC power output from the elements. Therefore, the DC-combining technique is crucial for effectively applying the rectifier array. Hybrid methods can indeed further improve DC conversion efficiency in specific cases. However, to achieve both wideband and efficiency simultaneously, hybrid methods require additional broadband matching networks, which typically increase the system's complexity. Complex circuits may introduce additional losses. DC combining can be implemented using series, parallel, or series-parallel configurations. In series DC combining, the efficiency decreases significantly with the addition of more units due to the voltage drop across each diode, and a failure in one component can lead to the entire array's failure. In contrast, the parallel configuration has a simple circuit structure, making it easy to implement. When the power and phase of multiple input signals are not perfectly aligned, the parallel configuration reduces losses and improves overall collection efficiency.

In this paper, we designed a rectenna and array systems, achieving significant improvements in low-power RF-to-DC conversion efficiency, bandwidth, and DC combining efficiency. In this study, our work represents an incremental advancement that improves key performance metrics:

(a) Bandwidth Optimization: By designing matching networks for the antenna and rectifier circuit, we extended the bandwidth to 1.2 GHz. This enhancement over existing energy harvesting technologies enables the system to cover a broader frequency range, harvesting more RF energy.
(b) Energy-Harvesting Efficiency: The optimized matching network in the rectifier maintains high rectification efficiency across the expanded 1.2 GHz bandwidth.
(c) Improved Omnidirectional Performance: Building on the omnidirectionality achieved in the *xoy* plane, we further optimized the *xoz* plane's performance, enabling effective omnidirectional energy harvesting in three-dimensional space.

Although this study represents an incremental improvement, we believe these enhancements are significant for practical applications. Our design achieves simultaneous advancements in omnidirectionality, bandwidth, and efficiency, providing a more competitive solution for three-dimensional energy-harvesting applications. This work offers valuable insights for the design of future technologies in this field. It can be applied for environmental RF energy harvesting in the Personal Communications Service (PCS), (1.85–1.99 GHz), WiMAXTM M2300T-01/02 (2.3–2.4 GHz), Bluetooth (2.4–2.48 GHz), and WiMAXTM M2500T-01 (2.5–2.7 GHz). The harvester strategically combines six microstrip rectenna elements with different directions and polarizations to enhance the stability of omnidirectional energy harvesting. Six elements use a parallel configuration to achieve high-efficiency DC combining. A compact rectenna employs impedance compression matching technology to achieve high-efficiency rectification under wideband and low-

power conditions. Finally, in a power density of 1 μW/cm^2, the harvester was rotated 360° to measure the DC output voltage at different frequencies.

2. Wideband Antenna Design

The layout and photograph of the wideband antenna are shown in Figure 1, with the top and back views, respectively. The top structure of the antenna consists of a 50 Ω microstrip line that feeds a trapezoidal radiator. The grounding section consists of a rectangular metal structure. The combination of the tapered trapezoidal radiator and the partial ground plane provides good impedance matching and achieves wideband performance. The substrate used is NPC-H220A produced by PILLAR Corporation in Osaka Japan, with a thickness of 0.8 mm. Its dielectric constant ε_r is 2.17, the loss tangent tan δ is 0.0004, and the overall dimensions of the antenna are 60.0 × 67.8 × 0.8 mm^3.

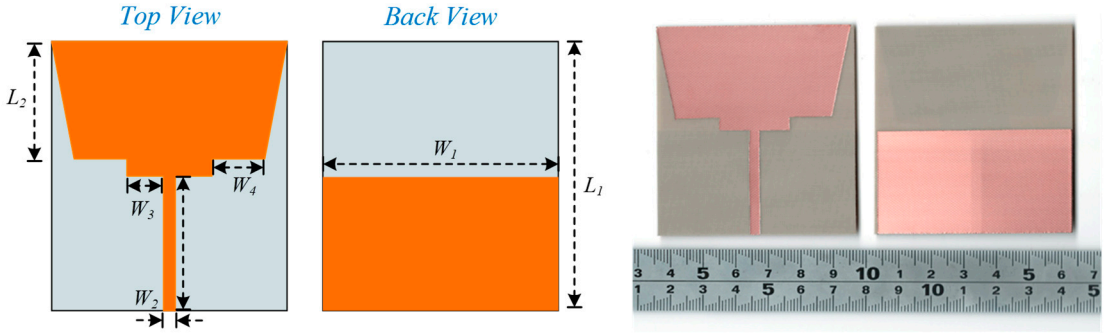

Figure 1. Layout and picture of the proposed antenna. (W_1 = 60 mm, W_2 = 2.9 mm, W_3 = 9.3 mm, W_4 = 13.4 mm, L_1 = 67.8 mm, L_2 = 29.6 mm).

Conventional microstrip patch antennas typically have narrow bandwidths, and their impedance characteristics are highly sensitive to the ground plane. To address these issues, a tapered trapezoidal radiator and a partial ground were are employed to achieve effective impedance matching and wideband performance. By adjusting the dimensions of the base and top edges of the trapezoidal radiator, the impedance distribution at the feed point could be optimized, enhancing the antenna's adaptability for practical applications. As shown in Figure 2, antenna structures with radiating patches in rectangular, circular, and trapezoidal shapes were compared. It was found that the trapezoidal patch exhibited the widest bandwidth and the best overall performance.

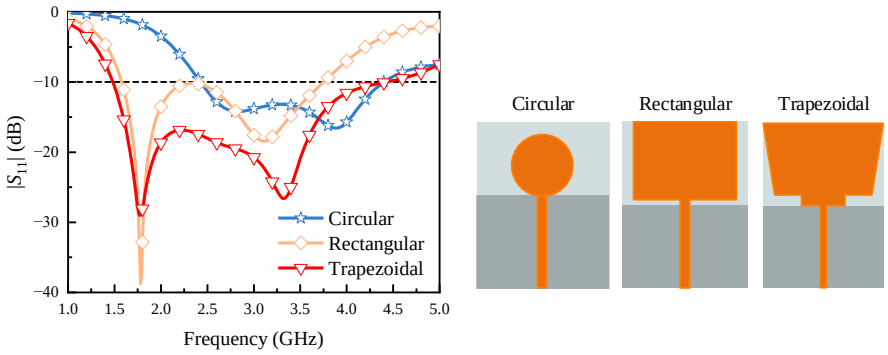

Figure 2. Comparing antennas with radiating patches in rectangular, circular, and trapezoidal shapes.

An Agilent vector network analyzer (Agilent N5242A) was used to measure the antenna's *S*-parameters, as shown in Figure 3. The N5242A Vector Network Analyzer is now manufactured by Keysight Technologies, which is also headquartered in Santa Clara, California, USA. The bandwidth with *S*-parameters below −10 dB in the measurement ranged from 1.5 GHz to 4.3 GHz, resulting in a bandwidth of 2.8 GHz. The experimental and simulated results aligned closely.

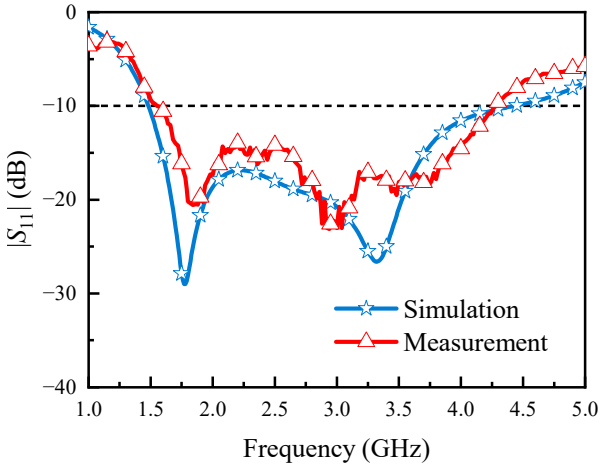

Figure 3. Measured and simulated $|S_{11}|$.

The measured and simulated radiation patterns of the antenna with the *xoz*-plane and *yoz*-plane are shown in Figure 4. The radiation patterns were tested in a microwave anechoic chamber. Measurements were conducted at 1.90 GHz, 2.35 GHz, 2.45 GHz, and 2.60 GHz. The maximum gains were measured at 1.87 dBi at 1.9 GHz, 2.6 dBi at 2.35 GHz, 3.5 dBi at 2.45 GHz, and 3.9 dBi at 2.6 GHz, respectively. The antenna exhibited good omnidirectional characteristics in the *xoz*-plane, with a 3 dB gain difference between 0° and 90° in the *xoz*-plane. In the *yoz* plane, the antenna exhibited a bi-directional radiation pattern, with radiation directed along both the $+z$ and $-z$ directions.

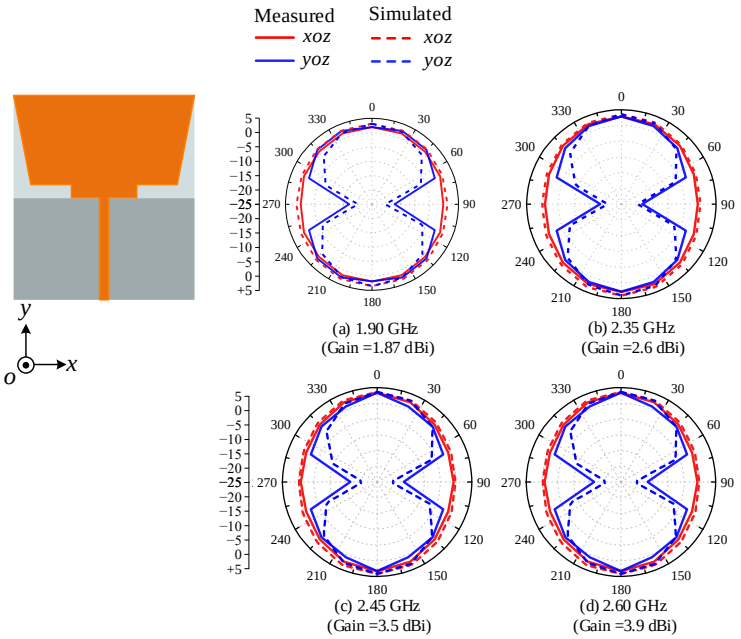

Figure 4. Measured and simulated radiation patterns at (**a**) 1.9 GHz, (**b**) 2.35 GHz (**c**), 2.45 GHz, and (**d**) 2.6 GHz.

3. Wideband Rectifier Design

The schematic of the wideband low-power rectifier is shown in Figure 5a. The circuit consists of a wideband matching network, an HSMS-285 diode, a DC-pass filter, and a DC load. In the wideband matching network, Part A is a short-circuited microstrip line. This reduces the imaginary component of the diode's impedance while leaving its real component unaffected. At low and high frequencies, the imaginary part of Z_{in1} is capacitive and inductive, respectively. Part B is a parallel open-circuit stub line. At high

frequencies, the electrical length of Part B is longer, causing Z_{in1} to rotate a greater distance on the constant conductance circle. At low frequencies, the electrical length of Part B is shorter, resulting in a smaller rotation distance for Z_{in1}. Ultimately, Z_{in1} is compressed, achieving impedance compression and reducing Z_{in1} variation with frequency. Part C is an impedance transformer that introduces a section of high-impedance line to match the circuit's total impedance to 50 Ω. These three components work together to optimize the circuit's wideband performance and impedance matching, ensuring effective wideband operation of the rectifier at low power levels. Figure 5b shows the $|S_{11}|$ of the rectifier with two different matching networks under −3 dBm power. The $|S_{11}|$ of the circuit with Parts A, B, and C is below −10 dB across the frequency ranges from 1.6 GHz to 2.7 GHz. In contrast, the circuit structure with only Part A has an $|S_{11}|$ below −10 dB in the narrower frequency ranges from 2.4 GHz to 2.6 GHz. It is evident that the combined effect of Parts A, B, and C significantly extends the bandwidth of the rectifier. As shown in Figure 5c, as the length of transmission line Part A increases, the frequency range gradually shifts toward lower frequencies. With the increase in length, the frequency moves further into the lower range, and the bandwidth gradually decreases, but the maximum efficiency improves. This is because achieving a wider bandwidth comes at the cost of sacrificing maximum efficiency. Nevertheless, a bandwidth of over 1 GHz can still be achieved. At higher power levels, by optimizing the matching network and selecting diodes suitable for different power levels, such as HSMS286 for 10 dBm and HSMS282 for 20 dBm, the circuit's application can be extended to a wider frequency band. As shown in Figure 5d, the simulation results indicate that the rectifier circuit with the Part A, B, and C structure can achieve a bandwidth greater than 1.4 GHz and an efficiency exceeding 50% under different power levels by using appropriate diodes.

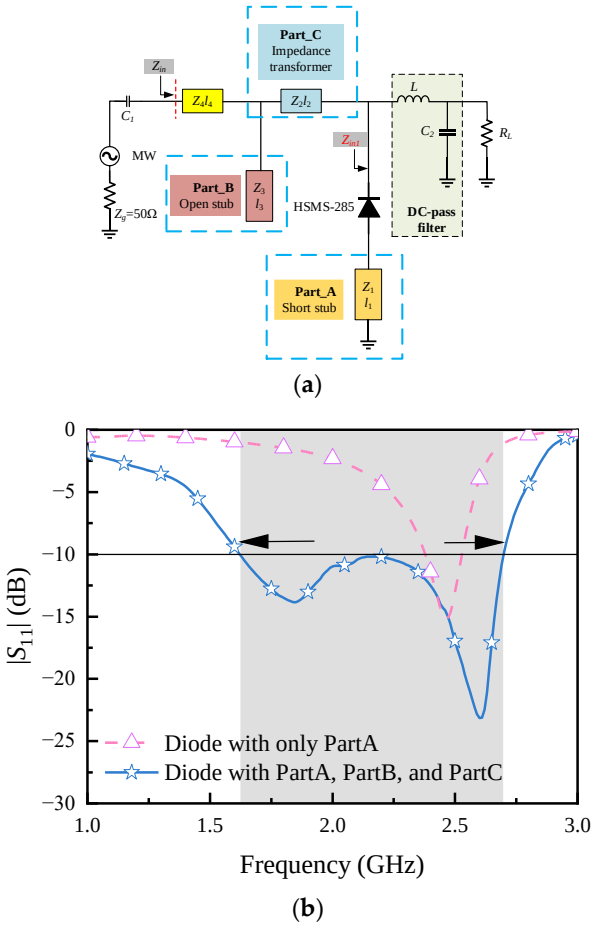

Figure 5. *Cont.*

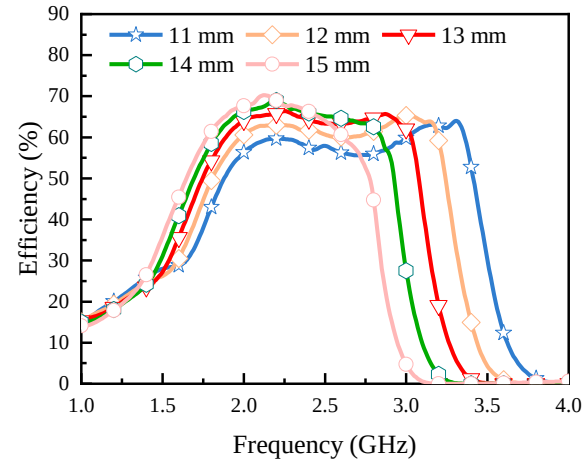

(**c**)

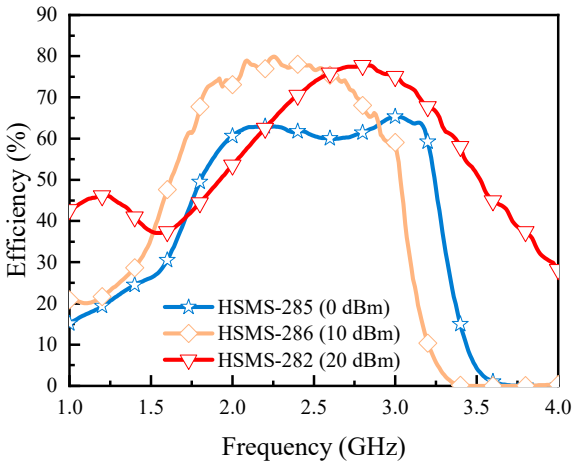

(**d**)

Figure 5. (**a**) Schematic of the wideband rectifier. (**b**) Comparison of $|S_{11}|$ for part A structure alone and for part A, B, and C structures at −3 dBm power. (**c**) The effect of varying the length of rectifier circuit Part A on the frequency. (**d**) Wideband rectification was achieved using Part A, B, and C structures with different diodes.

The layout with summarized parameters and a prototype of the proposed wideband rectifier are depicted in Figure 6. A 0.8 mm thick dielectric substrate, NPC-H220A, is used. The load used in the measurement is 820 Ω. The measured RF-to-DC conversion efficiency is presented in Figure 7, with a comparison to the simulated results. The frequency bandwidth with conversion efficiency over 50% spans from 1.50 GHz to 2.67 GHz at 0 dBm. Moreover, the maximum conversion efficiency of 67% is achieved at 2.45 GHz with an input power of 6 dBm. The reason for the discrepancy between the simulation and measurement is that the diode model used in the simulation may neglect certain non-ideal characteristics of real devices, such as parasitic inductance and capacitance, which can affect the high-frequency performance and conversion efficiency. Additionally, diode fabrication inconsistency and diode model mismatch cause the discrepancy.

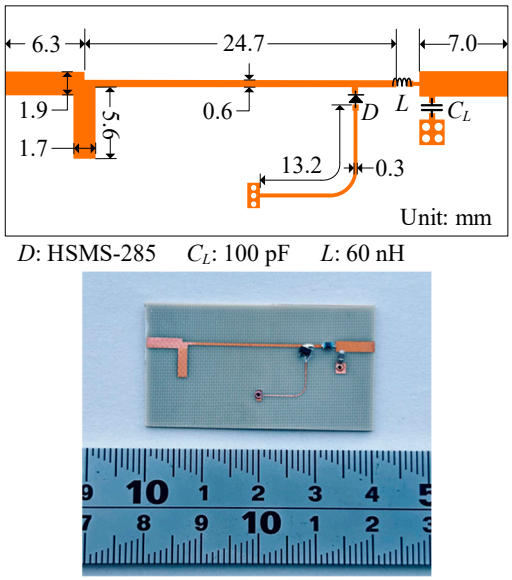

Figure 6. Layout and prototype of the proposed rectifier.

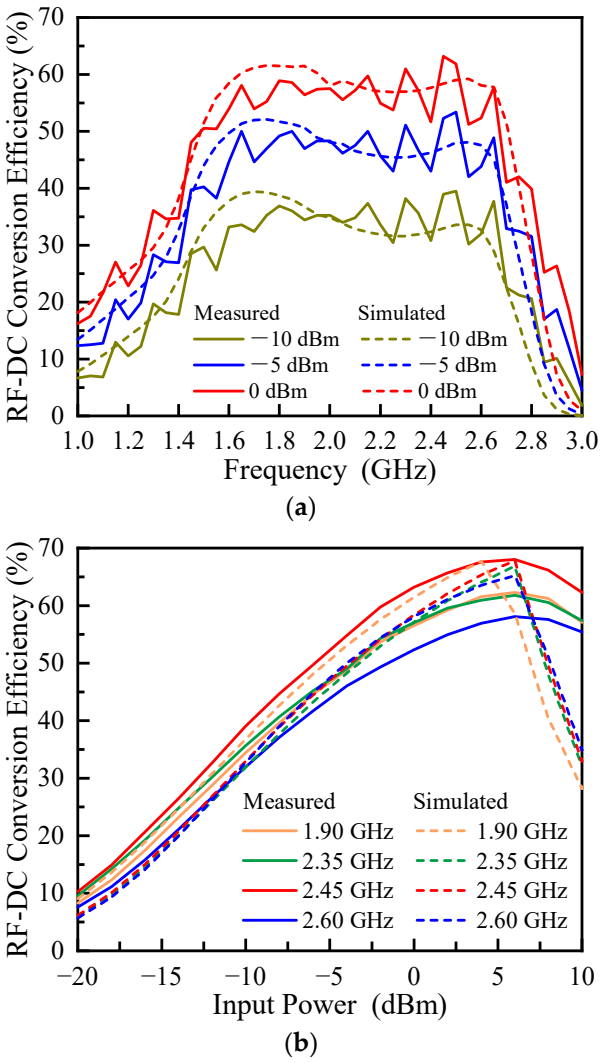

Figure 7. RF-DC conversion efficiency of the rectifier with (**a**) frequency and (**b**) input power.

The proposed wideband rectenna was fabricated and measured in an anechoic chamber, as presented in Figure 8a,b [4]. The signal generated by the RF signal generator (Agilent N5183A) was amplified by a power amplifier (PA) and transmitted through a standard horn antenna. A directional coupler, positioned between the PA and the horn antenna, was connected to a power meter (Agilent E4419B) to measure the transmitted power. The Agilent E4419B was manufactured by Agilent Technologies, headquartered in Santa Clara, CA, USA. The transmitting antenna and the rectenna were separated by a distance of 3 m. The available collected power P_r of the proposed rectenna was calculated using the Friis equation [5]:

$$P_r = \frac{P_t G_t G_r \lambda^2}{(4\pi D)^2} \quad (1)$$

where P_t is the input power of the transmitting horn antenna; G_t, and G_r are the gain of the horn antenna and proposed antenna, respectively; λ is the wavelength; and D is the distance between the transmitting and receiving rectenna (D = 3 m). The conversion efficiency is [7]:

$$\eta = \frac{V_{DC}^2}{P_r \times R_{load}} \times 100\% \quad (2)$$

where V_{DC} is the output voltage, and R_{load} is the DC resistance load with 820 Ω.

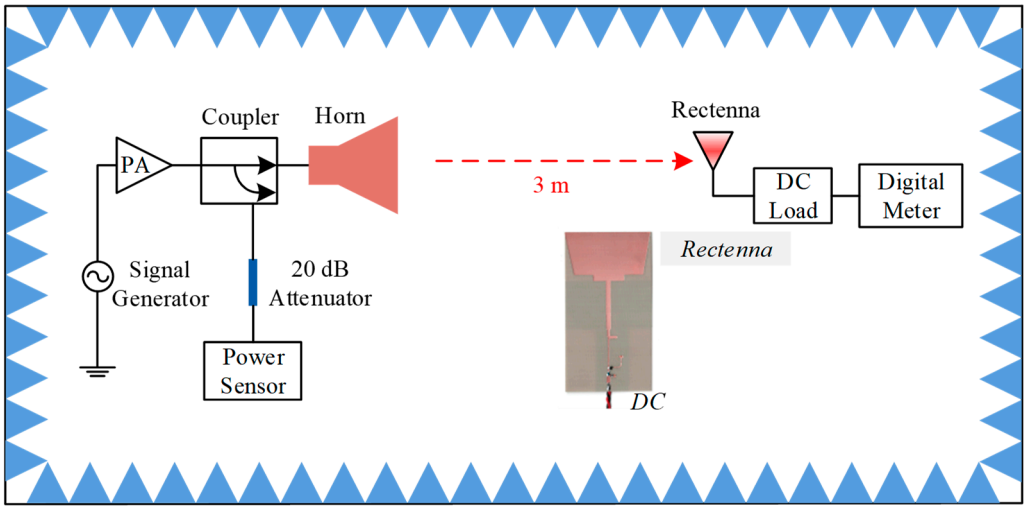

(**a**)

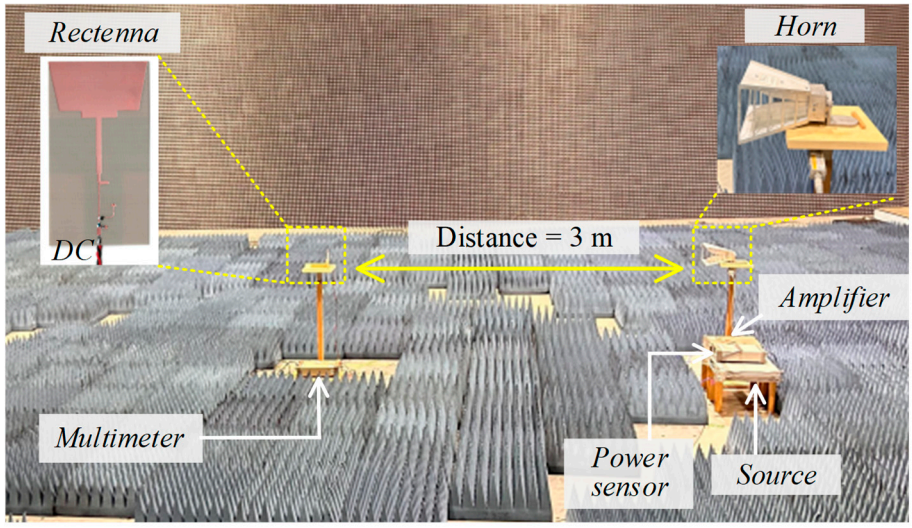

(**b**)

Figure 8. *Cont.*

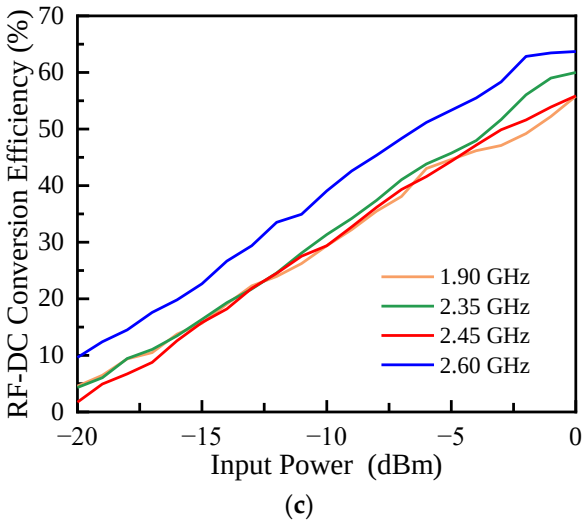

Figure 8. (**a**) Rectenna measurement setups; (**b**) measured in a microwave anechoic chamber; (**c**) measured conversion efficiency of the rectenna.

Figure 8c shows the measured conversion efficiencies of the rectenna at different input power levels. At an input power of 0 dBm, the maximum conversion efficiencies reach 55% at 1.90 GHz, 60% at 2.35 GHz, 55% at 2.45 GHz, and 65% at 2.60 GHz, respectively. RF-DC conversion efficiency decreases at lower power densities (<1 μW/cm^2). At very low input power levels, the driving voltage of the diode is insufficient to fully turn it on, leading to a significant reduction in rectification efficiency. To minimize the efficiency, drop under low power density conditions, we implemented the following measures: Selection of Low-Forward-Voltage Diodes: We chose diodes such as the HSMS285 or SMS7630, which are suitable for low-power applications. Wideband Impedance Matching Network: By employing impedance compression techniques and designing transmission lines A and Band C, we reduced the frequency dependence of the input impedance, extending the matching range and minimizing reflection losses at low power.

4. Fully Polarized Wideband Omnidirectional RF Harvester

As shown in Figure 9, the design of the harvester consisted of six elements, with two elements allocated for each polarization direction. Due to the 3 dB gain difference in the antenna's radiation pattern at 0° and 90°, we arranged two elements for each polarization direction, with a 90° angle between them to address this discrepancy. This arrangement allowed for more uniform energy reception from various directions, resulting in improved omnidirectional energy-harvesting performance.

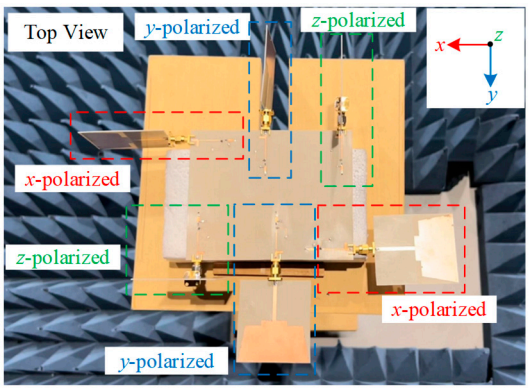

Figure 9. *Cont.*

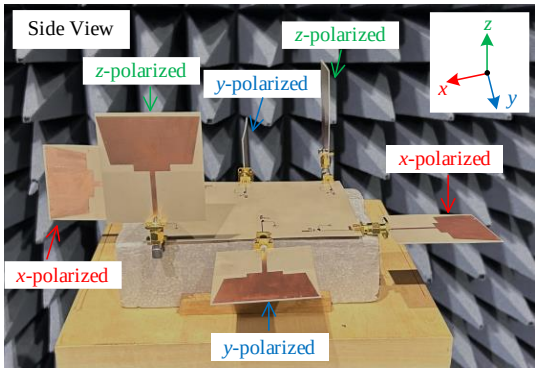

Figure 9. Wideband harvester with all-polarization and omnidirectional power harvesting.

To omnidirectionally harvest the environmental microwave power, each element exhibits varying characteristics in terms of power density, incident angle, and polarization direction. This variability may lead to energy loss due to the unstable DC power output from the elements. To address this problem, all elements are connected in parallel to improve the efficiency of the DC combining. The proposed array design offers the following features and advantages:

(a) Dual-plane omnidirectional coverage: Optimized array configuration achieves omnidirectionality in both the *xoy* and *xoz* planes.
(b) Full polarization: The design supports omnidirectional energy harvesting across three polarization directions (x, y, z), greatly expanding spatial coverage and polarization adaptability compared to existing single- or dual-polarization solutions.
(c) Wide bandwidth: Supporting up to 1.2 GHz bandwidth, the design enables simultaneous harvesting across multiple RF bands, capturing more environmental energy.

The equivalent circuit model of the DC combination for the rectifier array is shown in Figure 10a, where $R_{d0–d6}$ represents the impedance of the rectenna elements, and R_{L0} and R_L denote the loads of the individual elements and the rectenna array, respectively. The load of a single rectifier is R_{L0} = 820 Ω. Based on the parallel structure of the rectenna array, R_L is 137 Ω. The measurement procedure of the efficiency of the DC combining is described below [6].

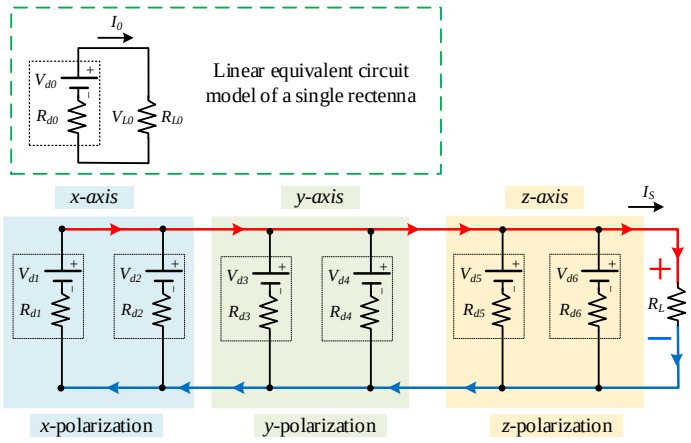

(**a**)

Figure 10. *Cont.*

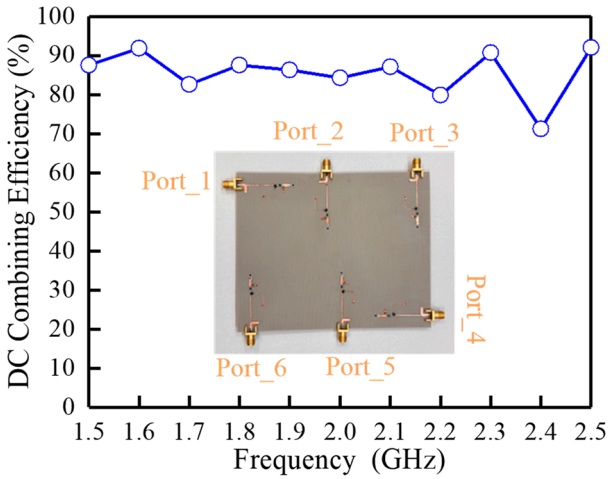

(**b**)

Figure 10. (**a**) The equivalent circuit for DC combination in the rectenna array. (**b**) DC combination efficiency.

(1) Each of the six rectifier elements is tested at an input power of 0 dBm, with the load (R_{L0}) 820 Ω, resulting in output powers P_1, P_2, …, P_6. Note that, when measuring the output power of each element, the others must be kept either open-circuited or short-circuited.
(2) Then, a power divider is employed to provide each element with 0 dBm. When the load (R_L) is 137 Ω, the resulting output power is P_{dc}.
(3) Finally, the efficiency of the DC combination is calculated as

$$\eta = \frac{P_{dc}}{P_1 + P_2 + \ldots + P_6} \times 100\% \quad (3)$$

The measured DC combining efficiency is shown in Figure 10b. Within the frequency range of 1.5 GHz to 2.5 GHz, the DC combination efficiency exceeds 70%. Notably, the maximum DC-combining efficiency achieved is 92%, with an energy loss of only 8%.

We positioned the harvester at the center of a rotating platform with a diameter of 6 m. The center-to-center distance between the transmitting antenna and the harvester was 3 m, and the load was 130 Ω. Under these conditions, the average power density S_{avg} on the harvester's surface was calculated by:

$$S_{avg} = \frac{P_t G_t}{4\pi D^2} \quad (4)$$

As shown in Figure 11, with a power density of 1 μW/cm^2, the harvester was rotated 360° to measure the DC output voltage at different frequencies. Figure 11a,b depict the DC output voltage of the harvester when the transmitting antenna is vertically and horizontally polarized. The harvester achieves omnidirectional power harvesting under various frequencies and polarization conditions. This demonstrates that the harvester collects power from all directions, validating its omnidirectional power-harvesting capability and design effectiveness.

A performance comparison between the rectenna and the related report is shown in Table 1. The design in [5] achieves omnidirectionality in a single plane but supports only single polarization, while the approach in [6] supports dual polarization but lacks sufficient omnidirectionality in the vertical plane. In contrast, our approach achieves omnidirectionality in both the *xoy* and *xoz* planes, supports triple polarization (*x*, *y*, *z*), and offers a bandwidth of 1.2 GHz. This comparison shows that the proposed harvester, which utilizes a parallel group array for DC combination, exhibits the highest efficiency at 92%. Therefore, compared to the currently published literature, the proposed omnidi-

rectional energy harvester offers the advantages of both wide bandwidth and high DC combination efficiency.

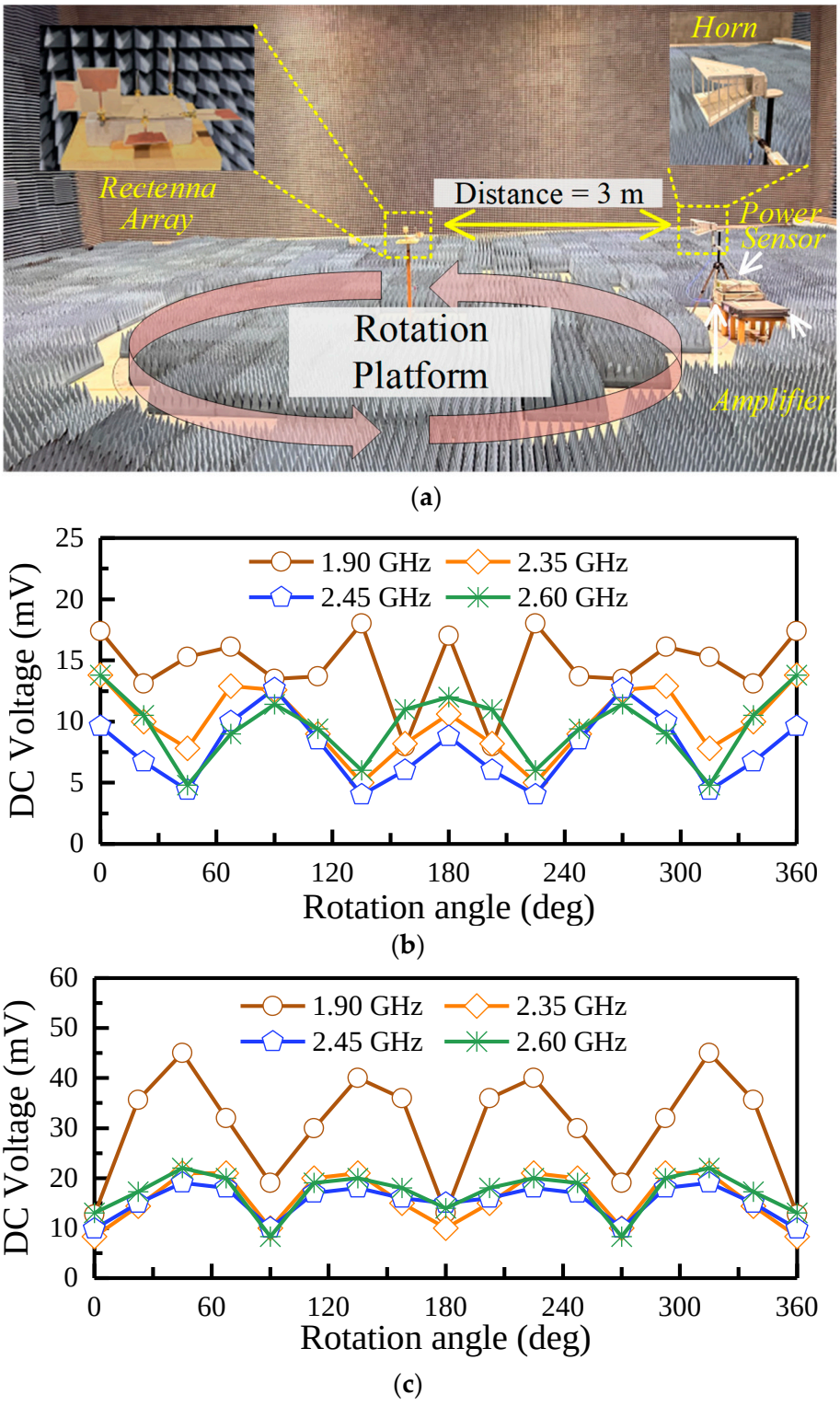

Figure 11. (**a**) Measured output DC voltages concerning rotation angle at 1 μw/cm^2, when the transmitting antennas are (**b**) vertically and (**c**) horizontally polarized.

Table 1. Performance comparison with the reported designs.

Ref.	Frequency (GHz)	Efficiency at 0 dBm	DC Combination Efficiency	Omnidirectional Power Harvesting	Polarization	Year
[4]	1.7–2.5	46%	N.A.	Two-dimensional	Full	2022
[5]	0.9, 2.45, 3.5	67%	N.A.	Two-dimensional	Single	2024
[6]	1.7–1.8, 2.1–2.7	70%	86%	Two-dimensional	Dual	2021
[7]	1.84	37%	N.A.	Two-dimensional	Dual	2018
This work	1.5–2.7	63%	92%	Three-dimensional	Full	2024

N.A. is Not Available.

5. Conclusions

In this work, we propose a fully polarized wideband omnidirectional RF energy harvester with a highly efficient DC combination. It can find applications in the places where Personal Communications Service (PCS), (1.85–1.99 GHz), WiMAXTM M2300T-01/02 (2.3–2.4 GHz), Bluetooth (2.4–2.48 GHz), and WiMAXTM M2500T-01 (2.5–2.7 GHz) operate. To enhance the stability of omnidirectional energy harvesting, the harvester integrates six rectenna elements with different directions and polarizations. In Section 2, the bandwidth of the antenna ranges from 1.5 GHz to 4.3 GHz, resulting in a bandwidth of 2.8 GHz. The antenna exhibits good omnidirectional characteristics. In Section 3, the proposed rectifier achieves over 50% RF-to-DC conversion efficiency across a 1.5 GHz to 2.7 GHz bandwidth at 0 dBm. In Section 4, the maximum DC combination efficiency of the rectifier array reaches 92%. For a power density of 1 $\mu W/cm^2$, the harvester was rotated 360° to measure the DC output voltage at different frequencies. These findings indicate that the harvester performs effectively with RF energy of all polarizations from various directions.

Author Contributions: Conceptualization, B.Y., J.J. and C.L.; methodology, J.J. and C.L.; software, J.J.; validation, J.J., B.Y., L.Y. and C.L.; formal analysis, J.J.; investigation, J.J.; resources, N.S.; data curation, J.J.; writing—original draft preparation, J.J. and L.Y.; writing—review and editing, J.J. and L.Y.; supervision, B.Y. and C.L.; project administration, B.Y. and J.J.; funding acquisition, B.Y., N.S. and C.L. All authors have read and agreed to the published version of the manuscript.

Funding: This work was supported in part by the Japan Society for the Promotion of Science, Grant-in-Aid for JSPS Fellows, under Grant 19J12459, and in part by the Collaborative Research Program of Microwave Energy Transmission Laboratory (MATLAB), Research Institute for Sustainable Humanosphere, Kyoto University. This work was also supported in part by the National Natural Science Foundation of China under Grant 62071316, and the Sichuan Science and Technology Program under Grant 2021YFH0152. NSFC U22A2015 and Sichuan Science and Technology Program under Grant 2024YFHZ0282.

Data Availability Statement: Data are contained within the article.

Conflicts of Interest: The authors declare no conflict of interest.

References

1. Shinohara, N. History and Innovation of Wireless Power Transfer via Microwaves. *IEEE J. Microw.* **2021**, *1*, 218–228. [CrossRef]
2. Guo, L.; Gu, X.; Chu, P.; Hemour, S.; Wu, K. Collaboratively Harvesting Ambient Radiofrequency and Thermal Energy. *IEEE Trans. Ind. Electron.* **2020**, *67*, 3736–3746. [CrossRef]
3. Wu, P.; Gao, S.-P.; Chen, Y.-D.; Ren, Z.H.; Yu, P.; Guo, Y. Harmonic-Based Integrated Rectifier–Transmitter for Uncompromised Harvesting and Low-Power Uplink. *IEEE Trans. Microw. Theory Tech.* **2023**, *71*, 870–880. [CrossRef]
4. Bo, S.F.; Ou, J.-H.; Dong, Y.; Dong, S.-W.; Zhang, X.Y. All-Polarized Wideband Rectenna With Enhanced Efficiency Within Wide Input Power and Load Ranges. *IEEE Trans. Ind. Electron.* **2022**, *69*, 7470–7480. [CrossRef]
5. Du, C.-H.; Cheng, F.; Yang, Y.; Zhu, H.; Gu, C. Omnidirectional Flexible Tri-Band Rectenna with Eliminated Matching Circuit for Ambient RF Energy Harvesting. *IEEE Trans. Microw. Theory Tech.* **2024**, 1–13. [CrossRef]
6. Song, C.; Lu, P.; Shen, S. Highly Efficient Omnidirectional Integrated Multiband Wireless Energy Harvesters for Compact Sensor Nodes of Internet-of-Things. *IEEE Trans. Ind. Electron.* **2021**, *68*, 8128–8140. [CrossRef]
7. Shen, S.; Chiu, C.-Y.; Murch, R.D. Multiport Pixel Rectenna for Ambient RF Energy Harvesting. *IEEE Trans. Antennas Propag.* **2018**, *66*, 644–656. [CrossRef]

8. Sun, H.; Guo, Y.-X.; He, M.; Zhong, Z. A Dual-Band Rectenna Using Broadband Yagi Antenna Array for Ambient RF Power Harvesting. *IEEE Antennas Wirel. Propag. Lett.* **2013**, *12*, 918–921. [CrossRef]
9. Olgun, U.; Chi-Chih, C.; Volakis, J.L. Investigation of Rectenna Array Configurations for Enhanced RF Power Harvesting. *IEEE Antennas Wirel. Propag. Lett.* **2011**, *10*, 262–265. [CrossRef]
10. Shen, S.; Zhang, Y.; Chiu, C.-Y.; Murch, R. A Triple-Band High-Gain Multibeam Ambient RF Energy Harvesting System Utilizing Hybrid Combining. *IEEE Trans. Ind. Electron.* **2020**, *67*, 9215–9226. [CrossRef]
11. Vandelle, E.; Bui, D.H.N.; Vuong, T.-P.; Ardila, G.; Wu, K.; Hemour, S. Harvesting Ambient RF Energy Efficiently With Optimal Angular Coverage. *IEEE Trans. Antennas Propag.* **2019**, *67*, 1862–1873. [CrossRef]
12. Kumar, M.; Kumar, S.; Bhadauria, A.S.; Sharma, A. A Planar Integrated Rectenna Array with 3-D-Spherical DC Coverage for Orientation-Tolerant Wireless-Power-Transfer-Enabled IoT Sensor Nodes. *IEEE Trans. Antennas Propag.* **2023**, *71*, 1285–1294. [CrossRef]
13. Wang, H.; Sun, S. An Omnidirectional CPW Leaky-Wave Antenna With Steering Conical Beam. *IEEE Antennas Wirel. Propag. Lett.* **2023**, *22*, 2042–2046. [CrossRef]
14. Battistini, G.; Paolini, G.; Costanzo, A.; Masotti, D. 3D-Printable Rectenna for Passive Tag Localization Exploiting Multi-Sine Intermodulation. In Proceedings of the 2023 IEEE/MTT-S International Microwave Symposium IMS 2023, San Diego, CA, USA, 11–16 June 2023; pp. 1077–1080. [CrossRef]
15. Du, F.; Cao, Y.; Xiu, X.; Che, W.; Xue, Q. Compact Dual-Band Shared-Aperture Base-Station Antenna Array Using Transparent Wideband Absorbing Metasurface and Radiator-Reused Scheme. *IEEE Trans. Antennas Propag.* **2024**, *72*, 2502–2512. [CrossRef]